BRIDGING THE GAP: DATA DRIVEN METHOD FOR LINEARIZED MODEL FIDELITY ENHANCEMENT

Marco Bergamasco
Technical Fellow
Leonardo Helicopters
Cascina Costa, Samarate, Italy

Matteo Mamino
Flight Mechanics Analyst
Leonardo Helicopters
Cascina Costa, Samarate, Italy

Giorgio Maisano
Flight Mechanics Specialist
Leonardo Helicopters
Cascina Costa, Samarate, Italy

ABSTRACT

Accurate flight dynamics models are necessary for cost and development time reduction in modern rotorcraft design. Yet, discrepancies frequently exist between high-fidelity, physics-based models and data-driven models identified from flight. Bridging this gap through physics-based model refinements often requires longer time frames than the tight development schedules allow. This paper presents a practical application of a data-driven Gain-Delay Correction Method (GDCM) to rapidly enhance the fidelity of a physics-based linearized rotorcraft model. The method optimizes a set of input and output gains and delays to address frequency responses discrepancies between linearized multi-body models and identified models derived from flight. This technique is applied the dataset of an AW family helicopter, covering a wide range of flight conditions. The results demonstrate that the method effectively identifies systematic gain discrepancies, for which a correction scheduled with airspeed is synthesized to improve the physics-based model accuracy. Also, a key limitation of the proposed approach is highlighted: the inability of a simple delay structure to compensate for phase underestimation in the physics-based model. The proposed workflow provides a pragmatic solution for rapid model fidelity improvement and offers a way to provide valuable cues to guide long term physics-based model refinements.

NOTATION

*

Symbols

COL Collective control position, %

J Cost function, -

J_{mag} Magnitude cost function, -

J_{phase} Phase cost function, -

H Helicopter linear time invariant model, -

LAT Lateral control position, %

LON Longitudinal control position, %

M_I Input gain-delay correction matrix, -

M_O Output gain-delay correction matrix, -

NX Longitudinal load factor, m/s^2

NY Lateral load factor, m/s^2

NZ Vertical load factor, m/s^2

P Roll rate, deg/s

PED Directional control position, %

Q Pitch rate, deg/s

R Yaw rate, deg/s

ROC Rate of climb, fpm

s Complex variable, rad/s

α Regularization factor

k Gain correction, -

τ Delay correction, s

ω Frequency, rad/s

*

Acronyms

CT-PBSID Continous Time Predictor Based Subspace Identification algorithm

GDCM Gain Delay Correction Method

ERF European Rotorcraft Forum

FCS Flight Control System

FLB FLIGHTLAB

LB Lower Bound

LTI Linear Time Invariant

UB Upper Bound

INTRODUCTION

In the development of rotorcrafts, accurate dynamic models are essential to predict and optimize vehicle capabilities, as well as to support and drive the design of a flight control system (FCS). Their use is now fundamental in any modern rotorcraft design and development process, as suggested in (Refs. 1, 10). In Leonardo, we employ various models for design purposes. These models can be grouped into two main categories: physics-based models and data-based models. The former are created incorporating helicopter data and systems models (e.g. rotors, fuselage, actuators, etc.) with physics-based mechanics and aerodynamics models. Commonly used software for the integration of physical models is FLIGHTLAB, a well-established product in the industry (Ref. 3). On the other hand, data-based models (referred to as CT-PBSID models) are directly derived from flight data using the Continuous-Time Predictor Based System IDentification algorithm (Refs. 7, 8).

Discrepancies in both root loci and frequency responses often arise between the physics-based and CT-PBSID models, and understanding the root causes of these differences may be challenging and require significant time and effort. As a result, considering the tight timelines associated with rotorcrafts development, traditional physics-driven model refinement approaches may sometimes be impractical. For this reason, this work applies a first-step methodology, referred to as Gain-Delay Correction Method (GDCM), aimed at addressing physics-based models frequency responses prediction deficits through a data-driven approach that prioritizes simplicity, rapid development, ease of implementation and, so, fast deployment.

While frequency response functions can be computed directly from flight data, this work utilizes CT-PBSID models as the reference data for the linearized physics-based model correction. CT-PBSID yields smoothed, noise-reduced, and consistent Linear Time-Invariant (LTI) models estimate that represent the underlying vehicle dynamics. These identified models provide a more stable and robust optimization target compared to raw, often noisy, frequency response functions from flight, ensuring the resulting corrections are not biased by windowing artifacts. In addition, another important advantage of CT-PBSID is to be able to use flight data collected entirely in closed-loop (i.e. with an active FCS), as it has been experimentally demonstrated in (Ref. 9).

References to the GDCM exist in the literature (Refs. 2, 6). However, these studies focus on the presentation of the method, rather than showing extensive practical applications, exploring its limitations or detailing the correction computation technique. In this article, the authors propose an example of how this technique can be applied, addressing some crucial aspects of the optimization step necessary to achieve usable model corrections. The approach is then tested on an extended rotorcraft dataset, demonstrating its potential to improve model fidelity in different flight conditions with a reduced deployment time.

PROBLEM STATEMENT

Given the LTI models $H_{FLB}(s)$ (i.e. the FLIGHTLAB linearized model of the bare rotorcraft) and $H_{CT-PBSID}(s)$ (i.e. the CT-PBSID model of the bare rotorcraft), both with $u(t) \in \mathbb{R}^m$ inputs and $y(t) \in \mathbb{R}^p$ outputs, the GDCM computes $M_I(s)$ and $M_O(s)$ that minimize frequency response differences between the two according to Eq. (1).

$$\min_{M_I(s), M_O(s)} \quad ||H_{CT-PBSID}(s) - M_O(s) H_{FLB}(s) M_I(s)||_D \quad (1)$$

$M_I(s)$ and $M_O(s)$ are defined in Eq. (2) as simple diagonal systems characterized by independent gains and delays across the various models input and output channels, while the formulation of norm $(|| * ||_D)$ is derived in the following section.

$$\begin{aligned} M_I(s) &= \begin{bmatrix} k_1^i e^{-\tau_1^i s} & & \\ & \cdots & \\ & & k_m^i e^{-\tau_m^i s} \end{bmatrix} \\ M_O(s) &= \begin{bmatrix} k_1^o e^{-\tau_1^o s} & & \\ & \cdots & \\ & & k_p^o e^{-\tau_p^o s} \end{bmatrix} \end{aligned} \quad (2)$$

PROPOSED APPROACH

As shown in Eq. (2) both $M_I(s)$ and $M_O(s)$ are diagonal gain-delay matrices. Each entry is written as $ke^{-\tau s}$, where k and τ represent the individual gain and delay correction values to be applied to each $H_{FLB}(s)$ input and output signal. An optimization procedure is set up to solve Eq. (1) by finding appropriate k and τ for each channel. Gains and delays optimization occurs in two distinct phases, leveraging on the independence of their effect on the open-loop response of the aircraft.

Let's define a matrix of input/output pairs, as in Eq. (3), that indicates which terms become optimization constraints and which terms are solely included in the optimization fitness function. The constrained terms are the ones corresponding to the what will be referred to as ”on-axis” responses in the section Optimization Setup.

$$DA = \begin{bmatrix} 0 & 1 & 0 & 0 \\ 1 & 0 & 0 & 0 \\ 0 & 0 & 1 & 0 \\ 0 & 0 & 0 & 0 \\ 0 & 0 & 1 & 0 \\ 0 & 0 & 0 & 1 \end{bmatrix} \tag{3}$$

Gain Computation

In this section, the details of the gains optimization algorithm are explained. Define the delta-gain matrix $\mathscr{G} \in \mathbb{R}^{p\times m}$ as

$$\mathscr{G} = \begin{bmatrix} G_{11} & \cdots & G_{1m} \\ \vdots & & \vdots \\ G_{p1} & \cdots & G_{pm} \end{bmatrix}, \tag{4}$$

where for each input $i \in [1, \cdots, m]$ and output $j \in [1, \cdots, p]$

$$G_{ij} = \operatorname*{median}_{\omega} \left(\frac{|H_{CT-PBSID}(i,j,\omega)|}{|H_{FLB}(i,j,\omega)|} \right). \tag{5}$$

$|H_*(i,j,\omega)|$ is the magnitude of the transfer function between input i and output j at frequency ω, where ω is considered over an adequate bandwidth in order to cover the system dynamics of interest.

Define input and output gain vectors as

$$\begin{aligned} k_I &= [k_{LON}\ k_{LAT}\ k_{PED}\ k_{COL}] \\ k_O &= [k_P\ k_Q\ k_R\ k_{NX}\ k_{NY}\ k_{NZ}]^T. \end{aligned} \tag{6}$$

Consider the product between the two gain vectors as $\mathbf{K} = k_O k_I$.

Finally, the non-linear constrained optimization problem for the gains can be defined as follows

$$\begin{aligned} &\min_{k_I,k_O} \|\mathscr{G} - \mathbf{K}\|_F^2 + \alpha \left\|k_O - \mathbf{1}_{p\times 1}\right\|_F^2 \\ &\text{s.t.} \quad \mathbf{K}(DA) = \mathscr{G}(DA), \\ &\qquad\quad k_O \wedge k_I \in [LB, UB] \end{aligned} \tag{7}$$

where α is the regularization term and $\mathbf{1}_{p\times 1}$ is a vector of ones of suitable dimension. The LB and UB are defined on the basis of the distribution of $|H_{CT-PBSID}(i,j,\omega)| \,/\, |H_{FLB}(i,j,\omega)|$ over the bandwidth of interest. The regularization term α is used to bias the algorithm toward modifying input gains rather than output gains. This preference is driven by physical reasons: any changes to the inputs will ripple through the entire simulated dynamics, while changes to the outputs have no effect on the evolution of the model internal states.

The constraint $\mathbf{K}(DA) = \mathscr{G}(DA)$ means that the product $\mathbf{K}$ must match the given matrix $\mathscr{G}$ on the subset of entries indexed by DA. Therefore, the most important input-output couples are enforced to be best matched at the expense of the others.

Delay Computation

In the following, the details of the algorithm for the delays estimation are outlined. Define the delta-delay matrix $\mathscr{D} \in \mathbb{R}^{p\times m}$ as

$$\mathscr{D} = \begin{bmatrix} D_{11} & \cdots & D_{1m} \\ \vdots & & \vdots \\ D_{p1} & \cdots & D_{pm} \end{bmatrix}, \tag{8}$$

where

$$D_{ij} = \operatorname*{median}_{\omega} \left(\frac{\angle H_{FLB}(i,j,\omega)}{\omega} - \frac{\angle H_{CT-PBSID}(i,j,\omega)}{\omega} \right). \tag{9}$$

$\angle H_*(i,j,\omega)$ is the phase in radian of the transfer function between input i and output j at frequency ω.

Define input and output delay vectors as

$$\begin{aligned} \tau_I &= [\tau_{LON}\ \tau_{LAT}\ \tau_{PED}\ \tau_{COL}] \\ \tau_O &= [\tau_P\ \tau_Q\ \tau_R\ \tau_{NX}\ \tau_{NY}\ \tau_{NZ}]^T. \end{aligned} \tag{10}$$

Consider the following combination of the delay vectors using the Kronecker product as $\mathbf{T} = \tau_O \otimes \mathbf{1}_{1\times m} + \tau_I \otimes \mathbf{1}_{p\times 1}$.

Finally, the non-convex non-linear constrained optimization problem for the delays can be defined as follows

$$\begin{aligned} &\min_{\tau_I,\tau_O} \|\mathscr{D} - \mathbf{T}\|_F^2 + \alpha \left\|\tau_O\right\|_F^2 \\ &\text{s.t.} \quad \mathbf{T}(DA) = \mathscr{D}(DA), \quad \tau_O \wedge \tau_I \in [0, UB] \end{aligned} \tag{11}$$

The UB is properly defined on the basis of the distribution of $(\angle H_{FLB}(i,j,\omega) - \angle H_{CT-PBSID}(i,j,\omega))/\omega$ over the bandwidth of interest. As before, the regularization term α is used to bias the algorithm toward modifying input delays rather than output delays.

The constraint $\mathbf{T}(DA) = \mathscr{D}(DA)$ means that the extended sum $\mathbf{T}$ must match the given matrix $\mathscr{D}$ on the subset of entries indexed by DA. Therefore, the most important input-output couples are enforced to be best matched at the expense of the others.

Results Example

The corrected LTI FLIGHTLAB model is referred to as $\hat{H}_{FLB}(s)$ and is computed according to Eq. (12).

$$\hat{H}_{FLB}(s) = M_O(s) H_{FLB}(s) M_I(s) \tag{12}$$

An example of the optimization results is reported in Figure 1 and Eq. (13) (where computed gain and delay corrections are expressed as functions of the parameters $\hat{k}$ and $\hat{\tau}$).

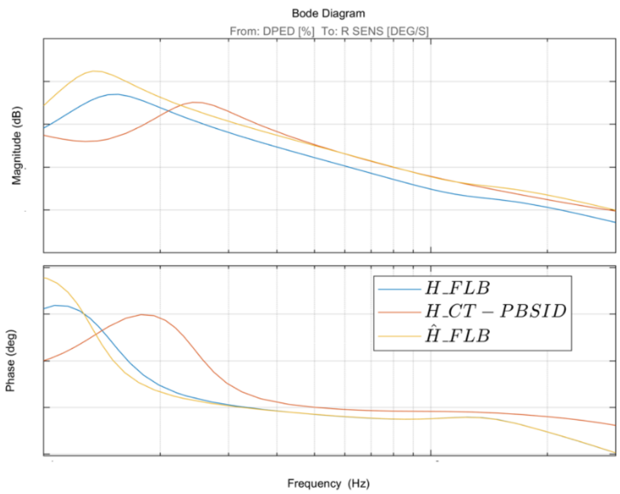

Figure 1. Example of the result of the presented method. Directional control position to yaw rate frequency responses of $H_{FLB}(s)$ (blue line), $H_{CT-PBSID}(s)$ (red line) and corrected $\hat{H}_{FLB}(s)$ (yellow line) are compared.

$$
M_I = \begin{bmatrix} \hat{k} & & & \\ & 0.817\hat{k} & & \\ & & \boxed{1.128\hat{k}} & \\ & & & 1.269\hat{k} \end{bmatrix}
$$

$$
M_O = \begin{bmatrix} 1.053\hat{k} & & & & & \\ & 0.746\hat{k} & & & & \\ & & \boxed{1.057\hat{k}} & & & \\ & & & 0.863\hat{k} & & \\ & & & & 0.890\hat{k}e^{-\hat{\tau}s} & \\ & & & & & 0.806\hat{k} \end{bmatrix} \tag{13}
$$

Finally, building on the results obtained across diverse flight conditions, the computed gains and delays are used to synthesize a model correction that is suited to be implemented in the FLIGHTLAB model.

Method Limitations

A main limitation of the GDCM is that no physical insight is given to the analyst about the cause of the models frequency responses discrepancies. Nevertheless, it may be argued that model corrections which are independent of flight conditions can be traced back to actuators non-linearities, sensors calibration errors, inadequate sensors dynamics modelling, lack of signals transport-delay, vehicle inertia errors. Conversely, corrections which exhibit non-negligible variations with respect to the flight condition may be a symptom of modelling deficiencies associated to specific flight regimes (e.g. errors in aerodynamics modelling). These cues may still be of use to the model developer to refine simulation model fidelity.

Also, as will be shown in the following sections, a clear limitation of this approach is that the $e^{-\tau s}$ structure with $\tau \geq 0$ can only add phase lag (delay) to the system. As a result, GDCM is not able to correct a model that already has lower phase (i.e., requires phase lead, or anticipation) with respect to the reference data.

At last, another limitation of the method is that the bare helicopter model root locus remains unchanged after the application of the correction (Ref. 6). As a result, physics-based model eigen-dynamics mispredictions cannot be tackled with GDCM.

RESULTS

Flight Conditions

The methodology exposed in the previous section was applied to a bare AW family helicopter. In total, 11 level flight conditions were included in the assessment, stretching across speed, altitude and weight ranges reported in Table 1.

Table 1. Nominal speed, altitude and weight of level flight conditions involved in the model correction synthesis.

Condition ID	Speed	Altitude	Weight
1	120 kts	Low	Low
2	140 kts	Low	Low
3	45 kts	Low	Low
4	120 kts	High	Low
5	45 kts	High	Low
6	60 kts	High	Low
7	90 kts	High	Low
8	120 kts	Low	High
9	140 kts	Low	High
10	60 kts	Low	High
11	90 kts	Low	High

Helicopter FLIGHTLAB Model

The AW helicopter physics-based, non-linear numerical model is developed within the FLIGHTLAB environment (Ref. 3). Main rotor aerodynamics are modeled using blade element theory coupled with a finite-state representation of the inflow (Ref. 4), while tail rotor aerodynamics employ a disk rotor model. Non-linear fuselage and tail surfaces aerodynamic loads are incorporated via high-fidelity look-up tables. Aerodynamic interference effects of the main rotor wake on the airframe are simulated using a finite-state dynamic wake interference model (Ref. 5). Servo-actuator dynamics are implemented with a parameter-based model tuned on experimental test data. Sensor dynamics and filtering characteristics are integrated according to the manufacturer-provided datasheet specifications.

Concerning system linearization, the full-order numerically linearized model has been consistently adopted throughout the analysis.

Helicopter CT-PBSID Models

As described in details in (Ref. 7), the data set for each condition is recorded during dedicated flights in which the pilot is

instructed to perform specific input command stimuli without the assistance of a stability augmentation system.
The main stimulus necessary for both helicopter system identification and frequency response computation is a frequency sweep. The task is particularly demanding for a human pilot because:

- it is performed without the stability augmentation system;
- while performing frequency sweep on a command axis the action on the rest of command axes should be kept at minimum or, at least, decoupled from the stimulated axis;
- during the task the helicopter should remain as close as possible to the trim condition.

Infringements of the aforementioned constraints can affect the accuracy of the dataset or even resulting in the data being unusable for identification purposes. Telemetry personnel and flight mechanics specialists are accountable for checking the constraints and eventually asking for a repetition of the flight condition if some of the former have not been observed.
The second set of stimuli, collected for validation purposes, consists of a series of doublets and step sequences (1-1-2-3) on each control channel.

Collected data are used to obtain the system frequency response functions and to identify the CT-PBSID models, as explained in (Ref. 8).

Optimization Setup

For each condition, the optimization process relies on multiple FLIGHTLAB linearized models, rather than a single one representative of the nominal flight condition. These additional models are obtained through the linearization of the model in perturbed trim conditions in the neighborhood of the nominal one. This approach serves two key purposes. First, the set of perturbed models is employed to explicitly identify potential model discontinuities in the neighborhood of the nominal condition (thus improving optimization robustness). Indeed, this may be the case for complex models that rely on a large amount of data. The second purpose is built upon the evidence that, in CT-PBSID models data gathering flights, the helicopter constantly displaces from the nominal trim condition (in response to identification stimuli). Hence, including perturbed FLIGHTLAB models in the algorithm serves to mirror this flight test feature, resulting in the optimizer being fed with a more complete and accurate physics-based representation of the helicopter small-amplitude response.
In the present application, perturbed linear models were computed accounting for perturbations of speed, rate of climb, and roll angle about the nominal trim condition. The magnitude of each perturbation was determined through visual inspection of flight data time histories, so to reflect the actual variations experienced by the helicopter in flight. In this way, the set of FLIGHTLAB LTI models is computed for each condition. Then, the optimization process selects the model that best represents the bundle and feed it to the optimization algorithm to synthesize the gain-delay corrections.

A similar approach is pursued for CT-PBSID models. For each condition, more than one CT-PBSID model is generally available. Also on this occasion, the process selects the most representative of the bundle to synthesize the gain-delay corrections.

It is worth mentioning that in condition 10, the nominal FLIGHTLAB linearized model and two perturbed models appeared to be outliers with respect to the bundle containing the remaining perturbed models, as outlined in Figure 2. This evidence stresses even more the need to include perturbed models in the development of whatever data-driven model correction. Nevertheless, as a result of visual inspection of all perturbed and nominal models frequency responses and root loci diagrams, it was determined that a dense bundle of consistent perturbed FLIGHTLAB models existed for each flight condition. As a result, all conditions listed in Table 1 were included in the study.

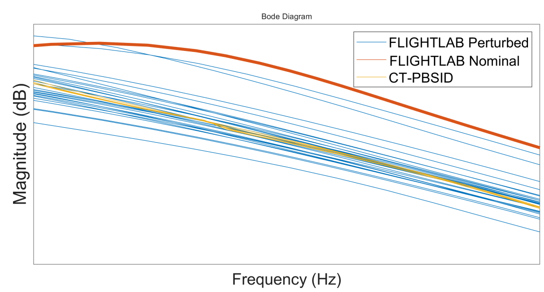

Figure 2. ***LON*** **to** ***Q*** **frequency response magnitude of nominal FLIGHTLAB (red), perturbed FLIGHTLAB (blue) and CT-PBSID models (yellow) associated to condition 10. The nominal model, together with two perturbed models, is an outlier with respect to the main bundle of perturbed models.**

The selection of on-axis frequency responses to be included as constraints in the optimization loop is marked with ”on” in Table 2 and was based on Leonardo company experience. In particular, on-axis responses deemed to be relevant for other systems design and/or verification activities involving linear flight mechanics models (e.g. FCS functions development) were involved in the optimization as constraints.

At last, concerning the remaining numerical settings, the frequency range considered in the optimization was adequately selected in order to consider the rigid body and the rotor dynamics of interest. Also, the regularization factor α was set to 1 in order to encourage the algorithm to prioritize adjusting input corrections.

Table 2. Summary of on-axis responses involved in the optimization as constraints.

	LON	*LAT*	*PED*	*COL*
P		**on**		
Q	**on**			
R			**on**	
NX				
NY			**on**	
NZ				**on**

Optimization Results and Correction Synthesis

The optimization results are shown in Figure 3 and Figure 4. For each condition and for each model input and output channel, the gain and delay corrections identified by the optimization algorithm are indicated by blue dots. In addition, a black dashed line represents the reference value of the null correction (i.e. 1 for gain corrections, as in Figure 3, and 0 for delay corrections, as shown in Figure 4).

The first notable finding relates to the delay corrections. As shown in Figure 4, only a few occasions produced non-zero delay corrections (such as the *NX* channel on condition 4). In contrast, the majority of cases resulted in null corrections. However, this outcome should not be interpreted as evidence of model accuracy; rather, it aligns with the known limitations of the GDCM. Based on the uncorrected FLIGHTLAB models comparison with CT-PBSID models, it appears that the FLIGHTLAB models consistently underestimate frequency responses phase values (as reported in the example in in Figure 5). Thus, the inability of the GDCM to introduce response anticipation explains the prevalence of null corrections. As a result, in the present application, the phase misprediction of the FLIGHTLAB model cannot be addressed.

With respect to gain correction results, no consistent trend is immediately apparent in Figure 3. On the other hand, gain corrections for a given channel appear scattered across the range of different conditions. However, a more informative perspective is obtained by examining the combined effect of input and output channels gain corrections (i.e. the product of the two) associated with specific frequency responses. Observing these composite corrections in relation to varying physical parameters among different conditions (such as airspeed, aircraft weight, or altitude) provides greater insight into the underlying correction behavior.

In Figure 6, the net gain corrections for on-axis frequency responses of Table 2 are reported as a function of airspeed. This representation reveals trends that were obscured when gain corrections were looked at individually on each channel.

Figure 6 highlights that at high speed (i.e. above 90 kts) regardless of the aircraft weight and altitude, the FLIGHTLAB model tends to underestimate the gain of *LON* to Q small amplitude response. This can be deduced based on the fact that above 90 kts, the product $k_{LON} \cdot k_Q$ is systematically greater than 1.

Concerning the *LAT* to P frequency response, the product $k_{LAT} \cdot k_P$ appears to be significantly close to 1 regardless of the condition. As a result, it may be concluded that little modeling improvement is likely to be obtained on the lateral axis with the gain-delay approach.

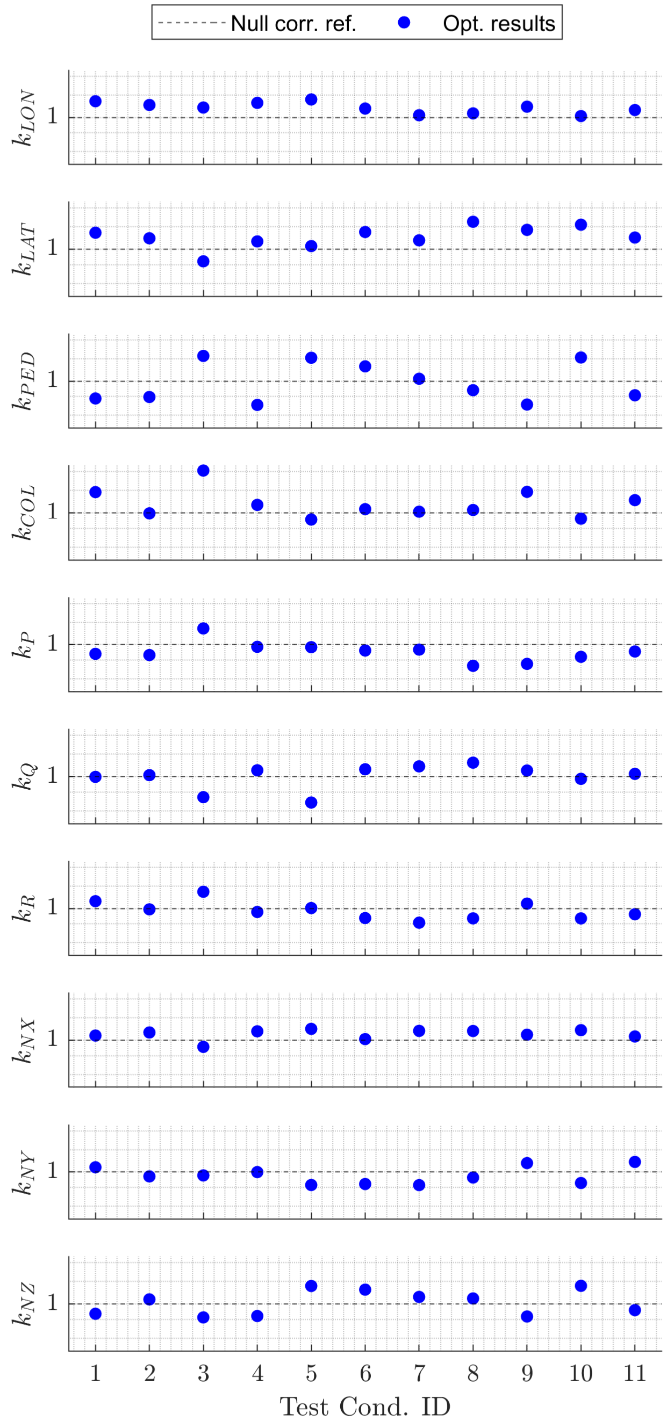

Figure 3. Gain corrections of each model input and output channel emerging from optimization results on each condition.

Moving to *PED* frequency responses, similar conclusions can be drafted from Figure 6 for *PED* to *NY* and *PED* to *R*. Indeed, $k_{PED} \cdot k_{NY}$ and $k_{PED} \cdot k_R$ reveal that the FLIGHTLAB model systematically underestimates small amplitude

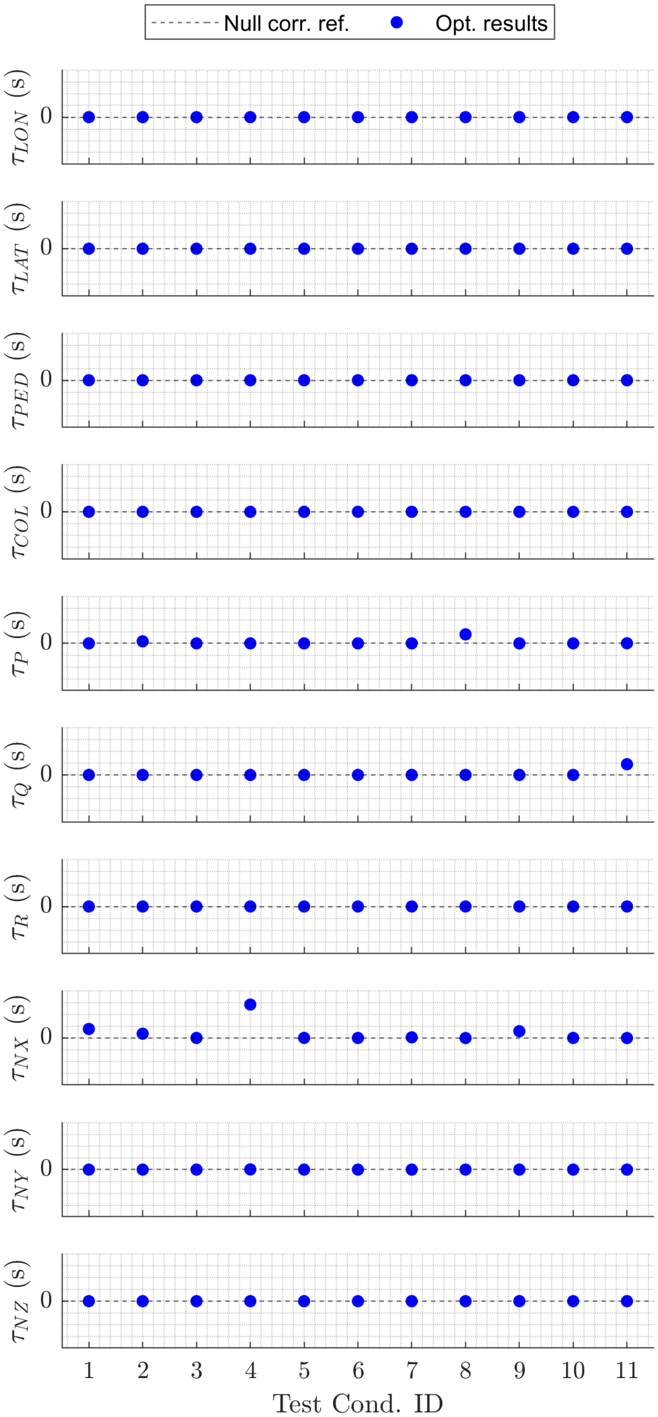

Figure 4. Delay corrections of each model input and output channel emerging from optimization results on each condition.

responses to *PED* at 45 kts (and, possibly, also at lower speeds). Conversely, opposite conclusions can be drafted for flight conditions above 120 kts, in which $k_{PED} \cdot k_{NY}$ and $k_{PED} \cdot k_R$ appear to be always smaller than 1.

At last, for what concerns the *COL* to *NZ* frequency response, $k_{COL} \cdot k_{NZ}$ appears systematically greater than 1 up to 60 kts. On the other hand, no particular trend emerges for greater

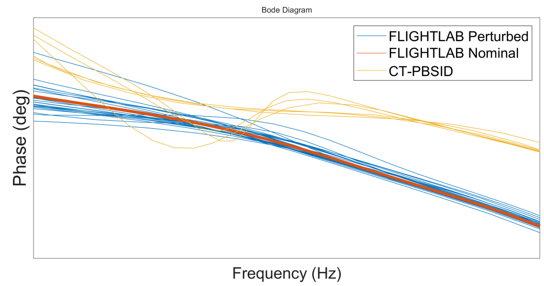

Figure 5. *PED* to *NY* frequency response phase of nominal FLIGHTLAB (red), perturbed FLIGHTLAB (blue) and CT-PBSID models (yellow) associated to on condition 3. FLIGHTLAB linear models consistently underestimate phase with respect to CT-PBSID models.

speeds.

It is worthy to observe that the insights offered by Figure 6 provide a compact yet informative basis for guiding the model developers in identifying potential physical model deficiencies that may account for the observed corrections. Ultimately, this understanding can support the replacement of data-driven corrections with physics-driven model improvements over the long term.

Building on these results, a model correction suitable for FLIGHTLAB implementation was synthesized. For what concerns gain corrections, a regression of the optimization results scheduled as a function of speed was derived for each model input and output channel. The net result of the FLIGHTLAB suitable correction on on-axis responses is compared to the optimization results in Figure 7. Conversely, in regards of delays, building on the aforementioned limitation of the GDCM for the present application, no correction was implemented.

Corrected Models Fidelity Improvement Assessment

The correction reported in Figure 7 was then implemented in the FLIGHTLAB model to carry out a frequency domain fidelity improvement assessment. The assessment was carried out in the same conditions used to derive the correction (i.e. conditions from 1 to 11 in Table 1) and against the same CT-PBSID models selected for the correction synthesis.

A revised version of the Tischler cost function J (Ref. 1), defined in Eq. (14) to (16), was exploited to assess model fidelity improvements.

$$J(H_M) = J_{mag}(H_M) + J_{phase}(H_M) \tag{14}$$

$$J_{mag}(H_M) = 20\, W_g \operatorname*{median}_{\omega} \left(|H_M(\omega)| - |H_{CT-PBSID}(\omega)|\right)^2 \tag{15}$$

$$J_{phase}(H_M) = 20\, W_p \operatorname*{median}_{\omega} \left(\angle H_M(\omega) - \angle H_{CT-PBSID}(\omega)\right)^2 \tag{16}$$

$W_g = 1$, $W_p = 0.0175$ and $H_M(\omega)$ is the physics-based model frequency response at frequency ω (i.e. either $H_{FLB}(\omega)$ or $\hat{H}_{FLB}(\omega)$). The median for this assessment was computed

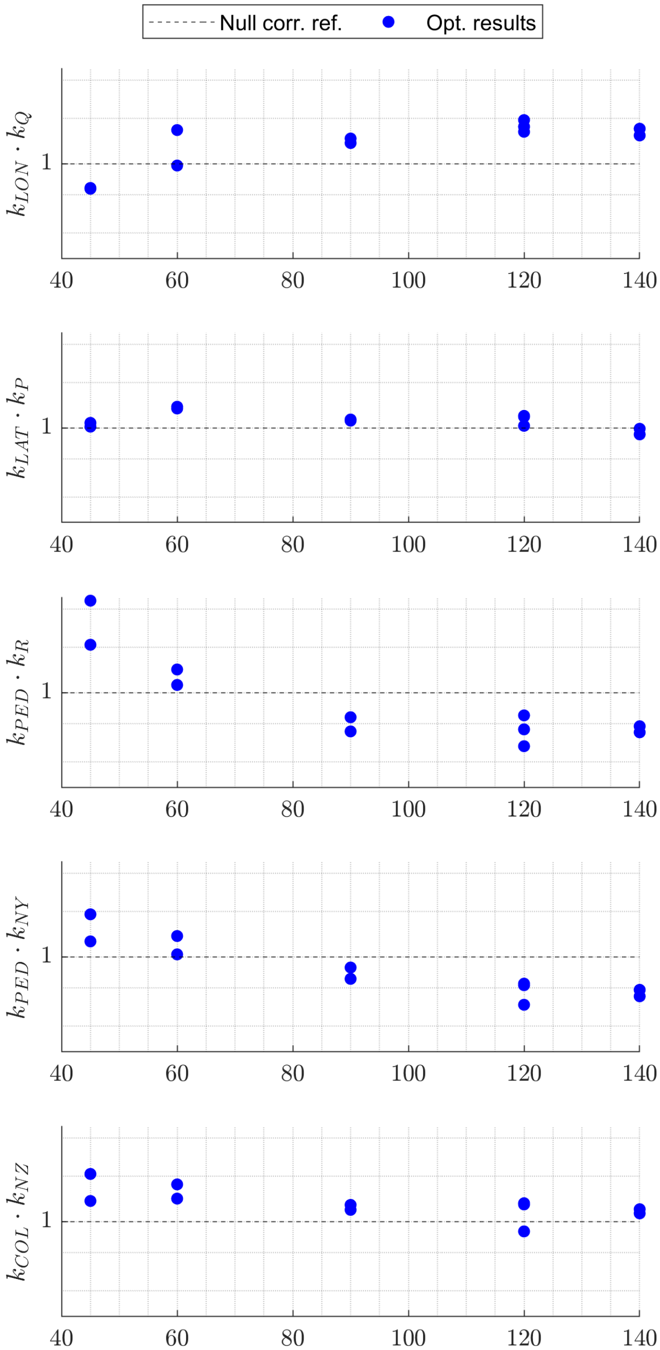

Figure 6. Effective gain corrections of on-axis frequency responses emerging from optimization results. The corrections are plotted as a function of aircraft speed.

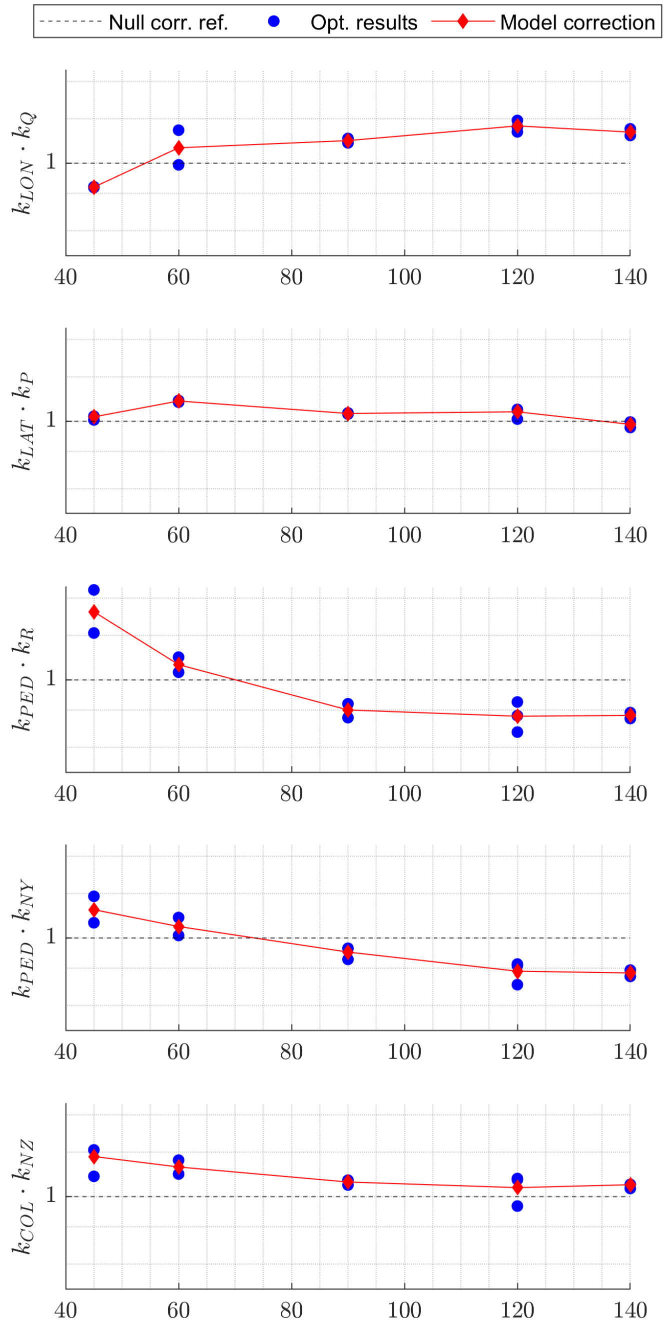

Figure 7. Net gain corrections of on-axis frequency responses resulting from FLIGHTLAB suitable correction (red line) and optimization results (blue dots).

over the same frequency range adopted in the optimization. In order to isolate model fidelity improvements, the ΔJ between the corrected ($\hat{H}_{FLB}$) and uncorrected (H_{FLB}) FLIGHTLAB models was computed according to Eq. (17).

$$\Delta J = J(\hat{H}_{FLB}) - J(H_{FLB}) \tag{17}$$

As a result, negative values of ΔJ are expected when the corrected FLIGHTLAB model exhibits improved prediction capabilities. In addition, in the figures, the ΔJ breakdown into magnitude and phase contributions (marked as ΔJ_{mag} and ΔJ_{phase}, respectively, and defined in Eq. (18) and (19)) is also reported.

$$\Delta J_{mag} = J_{mag}(\hat{H}_{FLB}) - J_{mag}(H_{FLB}) \tag{18}$$

$$\Delta J_{phase} = J_{phase}(\hat{H}_{FLB}) - J_{phase}(H_{FLB}) \tag{19}$$

This model improvement evaluation was limited to the nominal trim condition associated to each condition, with the aim of establishing whether (even on the same conditions used for model correction) fidelity improvements are to be expected on the nominal model. Indeed, the outcome of this analysis is relevant (for industrial applications of the model correction) and unapparent, meaning that the application of the model correction may still worsen the J metric of the nominal FLIGHTLAB model. This may be traced back to various reasons:

- the correction is computed based on a FLIGHTLAB model representative of the perturbed models bundle (and not on the nominal one);
- the applied model correction is not the exact one provided by the optimization, but rather a regression of the latter (as outlined in Figure 7);
- for off-axis responses, the optimization algorithm may end up worsening the model prediction capability in favor of improvements on the on-axis or other off-axis responses.

Finally, it is worth mentioning that condition 10 was excluded from this assessment, since (as outlined in Figure 2) the FLIGHTLAB nominal model turned out to lay outside of the bundle identified by perturbed models in this condition.

The improvements of FLIGHTLAB nominal models on on-axis responses (measured in term of ΔJ) are reported in Figures 8, 9, 10, 11, 12.

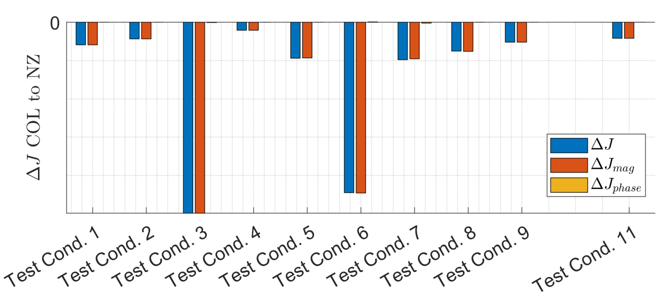

Figure 8. Improvements of corrected nominal FLIGHTLAB model on *COL* to *NZ* frequency responses with respect to the CT-PBSID model used for optimization.

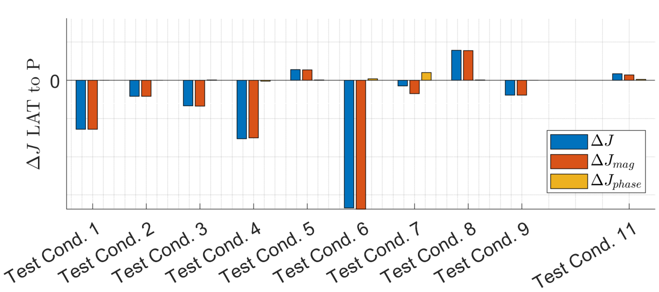

Figure 9. Improvements of corrected nominal FLIGHTLAB model on *LAT* to *P* frequency responses with respect to the CT-PBSID model used for optimization.

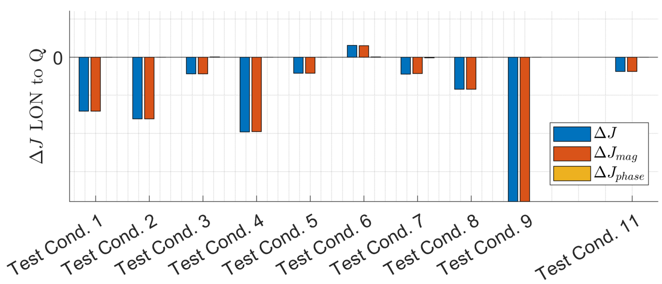

Figure 10. Improvements of corrected nominal FLIGHTLAB model on *LON* to *Q* frequency responses with respect to the CT-PBSID model used for optimization.

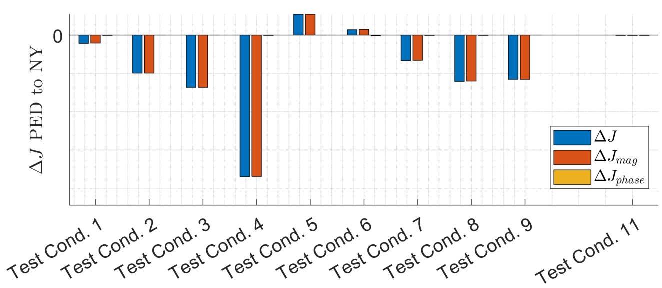

Figure 11. Improvements of corrected nominal FLIGHTLAB model on *PED* to *NY* frequency responses with respect to the CT-PBSID model used for optimization.

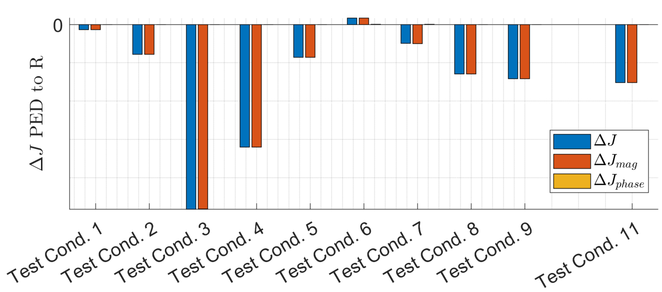

Figure 12. Improvements of corrected nominal FLIGHTLAB model on *PED* to *R* frequency responses with respect to the CT-PBSID model used for optimization.

First, as expected, Figures 8, 9, 10, 11, 12 exhibit numerically null values of ΔJ_{phase}. This evidence can be traced back to the fact that no delay corrections were implemented in the FLIGHTLAB model. As a result, being the delays the only correction component affecting frequency responses phase, J_{phase} remains unchanged.

On the other hand, considering ΔJ_{mag}, it appears from Figure 8 that *COL* to *NZ* always undergoes an improvement on corrected nominal FLIGHTLAB models. Also, it appears that flight conditions 3 and 6 exhibit the most significant model improvements. These conditions are some of the ones corresponding to the lowest speeds (i.e. 45 and 60 kts, as reported in Table 1) and associated to the most evident model prediction deficits (Figure 6). Nevertheless, it is worth mentioning that another low speed condition was included in the fidelity improvement assessment, i.e. condition 5 at 45 kts. However, while significant improvements are obtained on condition 3, only limited improvements are obtained on condition 5 (Figure 8). This evidence can be traced back to the fact that looking at the $k_{COL} \cdot k_{NZ}$ at 45 kts conditions in Figure 7, the correction implemented in FLIGHTLAB (red diamond) tends to be significantly closer to the top blue dot (i.e. optimization results for condition 3) rather than the bottom one (i.e. optimization results for condition 5). As a result, the implemented correction is more effective on condition 3 rather than on condition 5, since the latter appears to be overcorrected by the scheduling implemented in FLIGHTLAB. This feature also stands out on other axes responses and may occur at those speeds for which multiple, scattered optimization results are available. Indeed, since $J(\hat{H}_{FLB})$ is a non-linear function of the gain corrections, it may happen that the correction implemented in the FLIGHTLAB model undercorrects or overcorrects some conditions, also resulting, occasionally, in a deterioration of the model capability to predict on-axis responses.

As per *LAT* to *P*, similar conclusions can be drafted. Indeed, the majority of flight conditions experiences improvements from the application of the correction, and little to no nominal model prediction deterioration emerges from Figure 9. Also, the occurrences of minor deterioration (i.e. conditions 5 and 8) can be traced back to the same rationale discussed for *COL* to *NZ*. Indeed, condition 5 at 45 kts suffers the overcorrection driven by condition 3 (Figure 7) while condition 8 at 120 kts suffer the overcorrection driven by conditions 1 and 4 (Figure 7). At last, it is also worth observing that the most significant improvement is observed on condition 6 (60 kts), the same in which Figure 6 highlighted the most important prediction deficits for the uncorrected model.

Moving to *LON* to *Q*, substantial improvements are measured on almost all nominal models. In particular, conditions above 90 kts (where the baseline model exhibited the most significant prediction deficits, according to Figure 6) are the most positively affected by the model correction. The only occurrence of model deterioration is condition 6 (Figure 10). However, this result can be traced back to the conflicting information on $k_{LON} \cdot k_Q$ arising from conditions 6 and 10. As outlined in Figure 7, $k_{LON} \cdot k_Q$ exhibits two blue dots at 60 kts. However, one is greater than 1 (namely, optimization result on condition 10), while the other is smaller than 1 (i.e. optimization result on condition 6). The correction implemented in the FLIGHTLAB model (red diamond in Figure 7) computes a value for $k_{LON} \cdot k_Q$ which is greater than 1, driven by the outcome of the optimization on condition 10. As a result, condition 6 ends up with a gain correction opposite to the one computed by the optimizer.

At last, concerning *PED* to *NY* (Figure 11) and *PED* to *R* (Figure 12), improvements are measured on the majority of flight conditions. Indeed, great improvements are reported on conditions 3 (45 kts) and 4 (120 kts), which also exhibited the largest prediction deficits according to Figure 6. Also on this occasion, the minor model prediction deteriorations (present on condition 5 and 6) can be traced back to the same rationale discussed for *COL* to *NZ* and *LAT* to *P* responses.

In conclusion, based on the results obtained on corrected, nominal condition FLIGHTLAB linear models, it appears that the implemented correction generally improves the nominal FLIGHTLAB model prediction capability. It also appears that the correction is particularly effective on the largest model prediction deficits. However, when multiple, scattered optimization results are present for the same value of the correction scheduling variable, the corrected model may end up performing worse than the uncorrected one. Still, it remains unclear whether this evidence shall be traced back to the uncertainty of flight experiments, to limitations of the GDCM, to the choice of the (single) scheduling variable for the correction implemented in the FLIGHTLAB model or, most likely, to a combination of all the aforementioned. Hence, further investigations are required on this matter.

At last, for the sake of completeness, results on the most relevant off-axis responses are reported as well in Figures 13, 14, 15, 16, 17, 18, 19. However, as previously anticipated, little conclusions can be grasped on off-axis responses, since on top of all aforementioned considerations, the optimization algorithm may worsen the prediction capability of a response in favor of a greater improvement on another one.

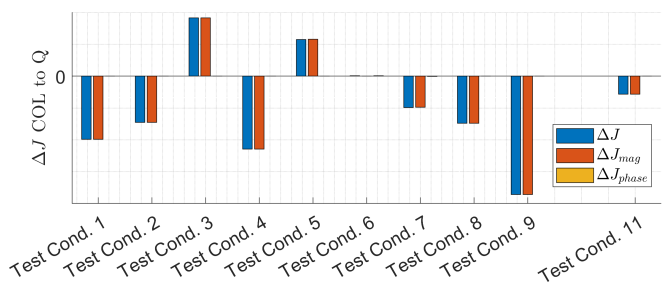

Figure 13. Improvements of corrected nominal FLIGHTLAB model on *COL* to *Q* frequency responses with respect to the CT-PBSID model used for optimization.

Figure 14. Improvements of corrected nominal FLIGHTLAB model on *COL* to *R* frequency responses with respect to the CT-PBSID model used for optimization.

CONCLUSIONS

This work successfully demonstrated the application of a Gain-Delay Correction Method (GDCM) to enhance the fidelity of a complex, physics-based rotorcraft model in a wide

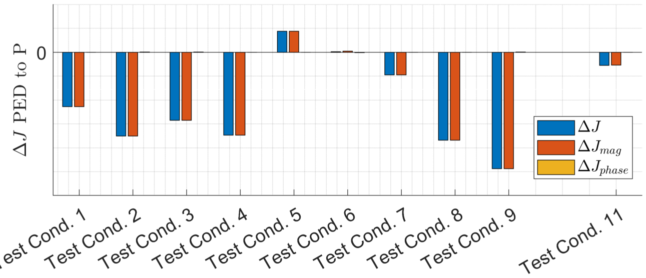

Figure 15. Improvements of corrected nominal FLIGHTLAB model on PED to P frequency responses with respect to the CT-PBSID model used for optimization.

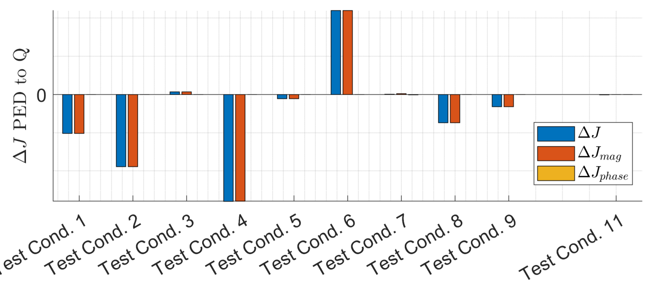

Figure 16. Improvements of corrected nominal FLIGHTLAB model on PED to Q frequency responses with respect to the CT-PBSID model used for optimization.

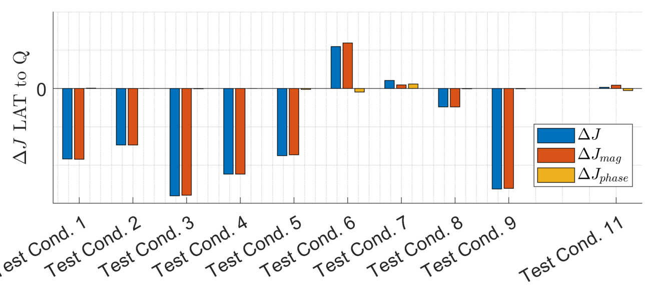

Figure 17. Improvements of corrected nominal FLIGHTLAB model on LAT to Q frequency responses with respect to the CT-PBSID model used for optimization.

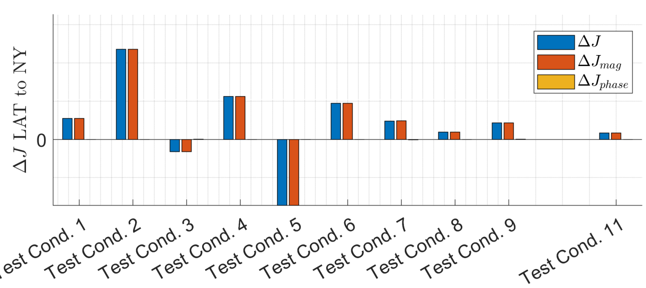

Figure 18. Improvements of corrected nominal FLIGHTLAB model on LAT to NY frequency responses with respect to the CT-PBSID model used for optimization.

range of flight conditions. The primary objective was to establish a rapid and robust data-driven workflow to reduce the

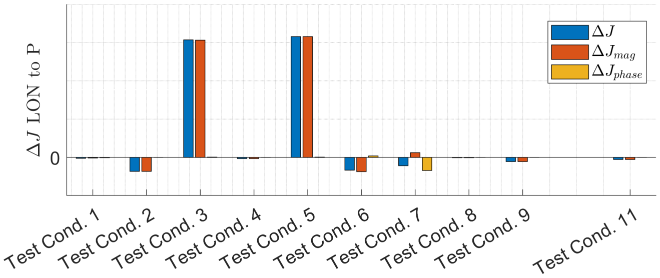

Figure 19. Improvements of corrected nominal FLIGHTLAB model on LON to P frequency responses with respect to the CT-PBSID model used for optimization.

discrepancies observed between the linearized, physics-based FLIGHTLAB model and data-based CT-PBSID models of an AW family helicopter.

The methodology, which optimizes independent gain and delay corrections for each model input and output, was systematically applied across 11 distinct level flight conditions. A key finding was that the simple delay correction proved insufficient for the present application, due to the baseline FLIGHTLAB models consistent phase underestimation. On the other hand, the gain correction returned valuable results; by analyzing the net gain corrections on on-axis responses as a function of airspeed, clear trends were identified.

Based on these findings, a gain correction scheduled as a function of airspeed was synthesized and implemented in the physics-based FLIGHTLAB model. A subsequent fidelity assessment confirmed that, on most occasions, the correction yielded tangible improvements in the model on-axis responses correlation with data-based models in the nominal flight conditions. Also, the correction was particularly effective in addressing the largest FLIGHTLAB model prediction deficits. However, when multiple optimization results were available for the same speed, the correction implemented in FLIGHTLAB occasionally failed to improve nominal model fidelity. No straightforward conclusion could be drafted, on the other hand, for off-axis responses.

The process also underscored the importance of using bundles of perturbed simulation models to ensure optimization robustness against model discontinuities (as in Figure 2).

While the GDCM does not offer direct physical insight into modeling deficiencies, its practical value is twofold. First, it provides a fast and effective mean of improving model fidelity for critical engineering applications. Second, the identified correction trends serve as valuable indicators for model developers, pointing towards specific flight regimes and dynamic responses where physics-based model improvements are most needed.

Future work could extend the corrected model validation to other flight conditions (that were not involved in the optimization) and explore more complex correction structures, such as first-order lead-lag filters, to address the observed phase discrepancies. Furthermore, the insights gained from this analysis can be of use to guide a more efficient physics-driven update of the FLIGHTLAB model.

Authors contact:
Marco Bergamasco, marco.bergamasco02@leonardo.com
Matteo Mamino, matteo.mamino@leonardo.com
Giorgio Maisano, giorgio.maisano01@leonardo.com

1. Tischler, M., and Remple, R., *Aircraft and Rotorcraft System Identification: Engineering Methods with Flight-Test Examples*, American Institute of Aeronautics and Astronautics, 2006.

2. Tischler, M.B., Berger, T., Ivler, C.M., Mansur, M.H., Cheung, K.K., and Soong, J.Y., *Practical Methods for Aircraft and Rotorcraft Flight Control Design – An Optimization-Based Approach*, American Institute of Aeronautics and Astronautics, 2017.

3. Val Du, R. W., and He, C., *FLIGHTLAB: A Suite of Rotorcraft Virtual Engineering Tools*, Rotorcraft Virtual Engineering Conference, Liverpool, UK, 2016.

4. He, C., *Development and Application of a Generalized Dynamic Wake Theory for Lifting Rotors*, Georgia Institute of Technology, Atlanta, GA, USA, 1989.

5. He, C., *Finite State Dynamic Wake Interference Modeling for Rotorcraft Simulation*, American Helicopter Society's 53rd Annual Forum, Virginia Beach, VA, USA, 1997.

6. NATO STO AVT-296 Research Task Group, *Rotorcraft Flight Simulation Model Fidelity Improvement and Assessment*, 2021.

7. Bergamasco, M., and Lovera, M., *Rotorcraft Model Identification: A Black-Box Time/Frequency Domain Approach*, 43rd European Rotorcraft Forum (ERF 2017), Curran Associates, 2017.

8. Bergamasco, M., and Lovera, M., *Identification of Linear Models for the Dynamics of a Hovering Quadrotor*, IEEE Transactions on Control Systems Technology, Vol. 22, (5), 2014, pp. 1696–1707.

9. Bergamasco, M., and Maisano, G., *Experimental Results on Closed Loop Helicopter Model Identification*, Vertical Flight Society's 81st Annual Forum and Technology Display (VFS 2025), Virginia Beach, VA, USA, 2025.

10. Bergamasco, M., and Cortigiani, N., Del Gobbo, D., Panza, S., Lovera, M, *The role of black-box models in rotorcraft attitude control*, 43rd European Rotorcraft Forum (ERF 2017), Curran Associates, 2017.

CLASSIFICATION & COPYRIGHT